

pubs.acs.org/cm Article

Transport in Twisted Crystalline Charge Transfer Complexes

Yongfan Yang, Yuze Zhang, Chunhua T. Hu, Mengmeng Sun, Sehee Jeong, Stephanie S. Lee,* Alexander G. Shtukenberg,* and Bart Kahr*



Cite This: https://doi.org/10.1021/acs.chemmater.1c04003



ACCESS

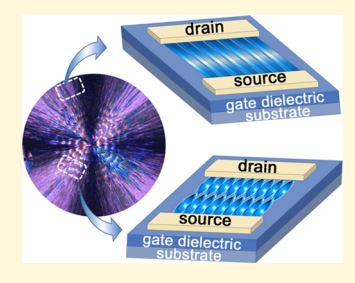
Metrics & More



Article Recommendations



ABSTRACT: Many crystals grow as banded spherulites from the melt with an optical rhythm indicative of helicoidal twisting. In this work, 23 of 41 charge transfer complexes (CTCs) are grown with twisted morphologies. As a group, CTCs more commonly twist (56%) than molecular crystals arbitrarily chosen in our previous research (31%). To analyze the effect of twisting on charge transport, three tetracyanoethylene-based CTCs with phenanthrene (PhT), pyrene (PyT), and perylene are characterized. PhT and PyT are subject to mobility measurements using organic field-effect transistors. The mobilities for twisted crystals are around three times higher than for crystals with no ostensible optical modulation, which are effectively straight. The differences in mobilities of straight and twisted crystals are considered computationally based on density functional theory. Straight crystal models built from crystallographic information files are



calculated and present anisotropic hole and electron transport. For twisted crystal models, adjacent layers in the supercell are rotated by 0.01° around experimentally determined twisting directions. The modified transfer integrals lead to a slight increase (up to 25%) in the calculated mobilities of twisted crystals. Comparisons of model calculations on individual fibrils and measurements of ensembles of fibrils indicate that interfaces between single crystals are likely consequential.

INTRODUCTION

Many fibrous molecular crystals spontaneously twist as they grow from the melt. Twisted fibrils typically branch in radial ensembles, or the so-called banded spherulites, displaying rhythmic optical properties as a consequence of continuous changes in crystallite orientation and refractivity.^{2,3} Recently, we analyzed 101 single component molecular crystals (corresponding to 155 polymorphs) and observed twisted growth from the melt in 31% under some conditions (large undercoolings, sometimes with viscosity-increasing additives). Included are pharmaceuticals such as aspirin and paracetamol, insecticides such as DDT and deltamethrin, as well as common laboratory compounds such as resorcinol9 and coumarin. 10

Here, we focus on a different class of molecular crystals, charge transfer complexes (CTCs) built from aromatic electron-rich donors and electron-poor acceptors. CTCs have a long history 11,12 and today are considered anew as active components of field-effect transistors, organic photovoltaics, and organic light emitting diodes. 13,14

CTCs are usually processed from solutions 15-17 to give high-quality films comprising millimetric domains and singlecrystalline ribbons. 18 Solvent-free techniques, like melt processing, more recently have been adopted to deposit both polymers and small organic molecules. 19-21 The deposition of CTCs as field-effect transistor active layers, however, still emphasizes solvent processing techniques. While several studies have characterized the microstructure of melt-processed CTCs, ^{22–24} the extraordinarily common twisted morphologies of CTCs grown from melt have not been described to the best of our knowledge.

The effect of twisting on charge transport was first investigated on twisted graphene bilayers whose electronic properties are remarkably sensitive to the azimuthal twist of one atomic layer to the next.²⁵ The study of the consequences of this angle is called *twistronics*, a name that embraces research on magic-angle graphene bilayers^{26–29} as well as other van der Waals heterostructures built from exfoliated 2D materials.³⁰ However, preparing materials with precise orientations of two layers just one-atom thick is challenging.²⁶ Crystals that spontaneously twist, albeit less than the magic angle of 1.1° between graphene layers, are thus worth investigating from the perspective of charge transport among other physical properties such as lattice dynamics. The easy preparation of CTCs and their common occurrence of twisting, prevent few obstacles in the search for the effect of comparatively modest twists on electrical properties.

In this work, we surveyed the crystallization of CTCs from the melt and found an even greater propensity (23/41 = 56%)of twisted morphologies compared to monocomponent systems. Three 1:1 mixed-stack tetracyanoethylene (TCNE)based CTCs with phenanthrene (PhT), with pyrene (PyT),

Received: November 22, 2021 Revised: January 11, 2022



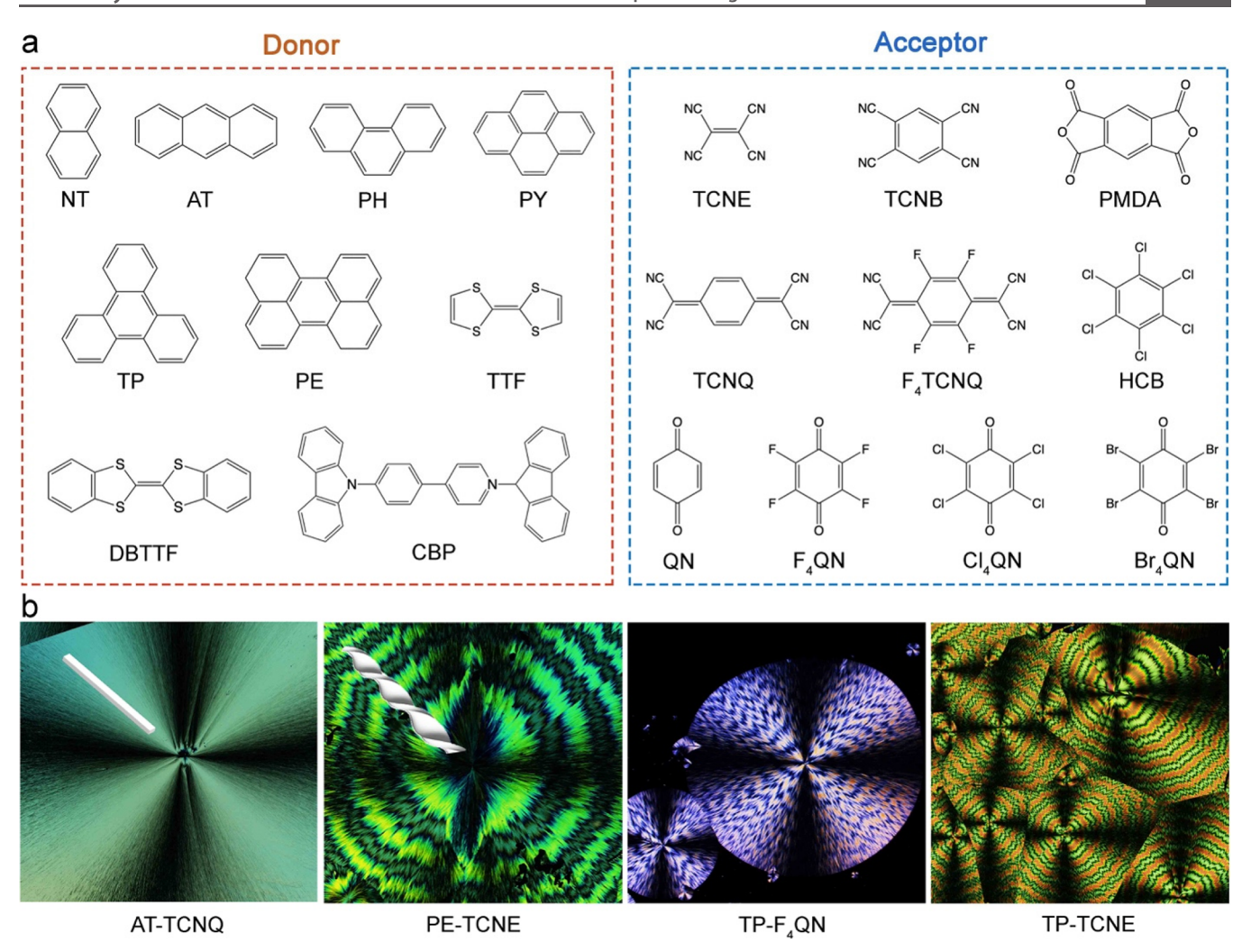


Figure 1. (a) Donors and acceptors used for the synthesis of CTCs. (b) Optical images of one straight and three twisted CTCs between crossed polarizers.

and with perylene (PeT) were characterized in greater detail. Charge transport in PhT and PyT films with straight and twisted crystals grown from the melt was measured using organic field-effect transistors (OFETs). The carrier mobilities of transistors comprising twisted crystals turned out to be three times higher than those comprising straight crystals. Model calculations based on density functional theory (DFT) predicted only a slight (several percent) increase in mobility of individual twisted crystals. The CT enhancement likely arises in the packing of ensembles of crystals in spherulites that are not captured in the calculations, but which nevertheless provide a base estimate of the consequence of twisting a single crystal.

RESULTS

Common Occurrence of Twisting in CTCs. Nine common donors and ten acceptors (Figure 1a) were chosen for the synthesis of binary CTCs. The details of the CTCs synthesis and the growth of straight and twisted crystals from the melt are given in the Experimental Section. Some combinations between donors and acceptors cannot form CTCs or the synthesized CTCs decompose before melting. The results for the 41 available CTCs are summarized in Table S1. The crystal structures of most substances were characterized previously and that of six new CTCs were determined

here by single-crystal X-ray diffraction (Supporting Information) and summarized in Table S2. Twisting was evidenced as the rhythmic variations of absorbance and retardance observed using a polarized light microscope because of the progressive change in crystallite orientation along the fiber elongation direction (Figure 1b). "Straight crystals" present the same optical orientation along the length of the fiber and no change of retardance observed under polarizers. Crystals with very large pitches are effectively straight. The fraction of CTCs that twist, 23/41 = 56%, is much higher than arbitrarily selected single component molecular crystals: 130/480 = 27% reported by Bernauer¹ and 48/155 = 31% in our recent study.⁴ Such a high percentage of twisting in CTCs is statistically robust because if the probability of twisting in a randomly selected crystalline compound is equal to 0.3, the binomial formula predicts that the likelihood of observing twisted morphologies in 23 materials of 41 compounds is vanishingly small, 4×10^{-6} .

The statistically meaningful differences in twisting frequency among CTCs (0.56) and arbitrarily selected monocomponent compounds (0.31) may be attributed to a narrower range of CTC crystal structure types. In particular, 35 of 41 CTCs have 1:1 stoichiometries and crystallize in a mixed-stack mode with alternating donors and acceptors in columns. Although the mutual orientation of molecules varies, the similarity in the

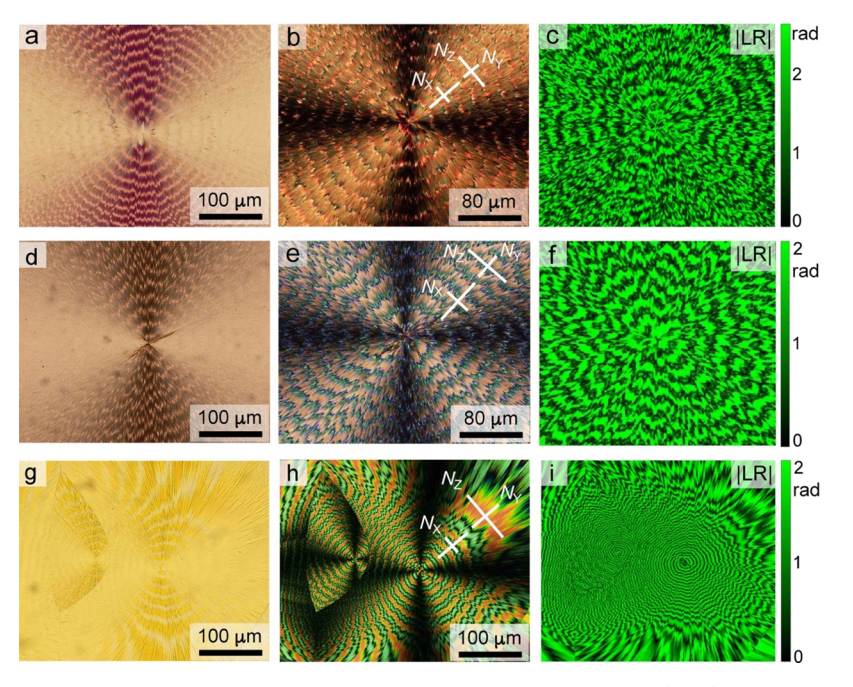


Figure 2. Banded spherulites of PhT, PyT, and PeT viewed under a horizontally oriented polarizer (a,d,g), between crossed polarizers (b,e,h), and linear retardance (ILRI) imaged by Mueller matrix polarimetry for PhT (c) at 700 nm, for PyT (f) and PeT (i) at 550 nm.

overall packing mode may be a factor enabling these CTCs to twist.

Crystal Structures and Optics of Three TCNE-Based CTCs. Three 1:1 mixed-stack TCNE-based CTCs with PhT, with PyT, and with PeT were characterized in greater detail, a series of twisted crystals with increasing annellation of the donors. The crystal structures of PyT (Refcode PYRCYE10³¹) and PeT (Refcode PERTCE10³²) were published in the 1960s. Here, their structures were redetermined and the structure of PhT was added (Table S2). All three CTC crystals have the 1:1 donor:acceptor mixed-stack configuration. Stacks run along the crystallographic a-axis for PhT and PyT, and b-axis for PeT (Figure S1). In each case, the mean planes between donors and acceptors are near parallel (PhT = 1.1°, PyT = 3.4°, and PeT = 1.8°) with the distances between their mean planes being 3.27, 3.35, and 3.39 Å, respectively. Hirshfeld surface analysis with two-dimensional fingerprint plots^{33,34} in Figure S2 emphasize donor-acceptor $\pi \cdots \pi$ interactions and C-H···N hydrogen bonds between molecules.

Twisted PhT and PyT crystals grew as banded spherulites from melts at 50-80 °C, and twisted PeT grew at <10 °C in dry ice. In these cases, no additives were necessary to induce twisting. Spherulites composed of straight crystallites grew at temperatures about 20 °C higher in each case (Figure S3). As shown in Figure 2, after some distance from the core, twisted fibrils grew radially from a central nucleus and displayed concentric rings of varying linear retardance with a pitch of about $20-50~\mu{\rm m}$. Between crossed polarizers, the birefringence oscillates between $n_Y-n_X=0.074$ and $n_Z-n_Y=0.130$ for PhT at 700 nm, 0.044 and 0.017 for PyT, and 0.096 and 0.033 for PeT at 550 nm.

Generally, the local structures of straight and twisted crystals from melts are comparable as indicated by powder X-ray diffraction (Supporting Information) and Raman spectroscopy (Supporting Information). Meanwhile, their electronic structures are comparable as evidenced by the energies and polarization of the visible light absorption spectra. As shown

in Figure S4, both straight and twisted crystals grown from melts present the same powder X-ray diffraction patterns. Also, the diffraction patterns were consistent with those of solution-grown crystals and single crystals. Raman spectra supported the same crystal structures for both straight and twisted crystals (Figure S5).

The fiber elongation directions were determined as <010> for both straight and twisted PhT and PyT (i.e., n_Y) by analyzing preferred orientations observed in 2D X-ray diffraction patterns collected from the as-grown films. PeT fibers in spherulites decomposed at the melting temperature (~270 °C), complicating the X-ray diffraction analyses. PeT will be carried forward in computational investigations based on single-crystal structure analysis, but not in experiments. The fiber elongation along the a-axis (n_Y ||<100>) was deduced by comparing the linear dichroism of fibers in spherulites (Figure 2g) to single crystals (Figure S1h, S1i) for which 2D X-ray diffraction characterization was possible. Solution-grown crystals of PhT and PyT formed {001} plates, while PeT grew as <010> needles (Figure S1).

Straight and twisted crystals showed comparable polarized absorption spectra with the characteristic peak λ_{max} = 520 nm for PhT, 510 nm for PyT, 35,36 and 410 nm for PeT, respectively (Figure S6). Compared with the melt-crystallized films, the solution-processed single crystals show almost the same characteristic peaks λ_{\max} except for PeT. The absorbance λ_{max} varied between solution and melt grown PeT crystals only because of decomposition. The crystals show high absorbance when the polarized light is parallel to the donor-acceptor stacking (A_{\parallel}) , a-axis for PhT and PyT and b-axis for PeT (the tangential direction in the banded spherulites in Figure 2a,d,g), but low absorbance in the orthogonal orientation $(A_{\perp})^{3}$ measured using a CRAIC Technologies 508 PV microspectrophotometer. The dichroic ratios A_{\parallel}/A_{\perp} were 8.1, 9.2, and 3.5 for solution-processed crystal films of PhT, PyT, and PeT, respectively.

Mueller matrix imaging polarimetry 38-42 (Supporting Information) was used to quantify the linear retardance (I LRI) and circular retardance (CR) of twisted crystals. As shown in Figure 2c,f,i, the |LR| oscillates along the growth direction from 0 to 2 radians for the film thickness around 2 μ m. A CR signal is strong in some cases, even though all the TCNE complexes are centrosymmetric. Optical activity of a kind can arise in polarimetry because a material is optically inhomogeneous along the light path. CR may result from misoriented, overlapping anisotropic lamellae, a kind of optical activity associated with the mesoscale stereochemistry of the refracting components.^{5,43} Neither chiral molecules, nor chiral space groups are required. Opposite twists can arise from enantiopolar growth of branches emanating from centric crystallites at the nucleus. PeT for instance (Figure 3) shows heterochiral domains that are effectively dextro- and levorotatory.

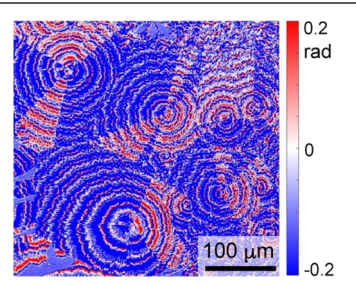


Figure 3. Circular retardance (CR) of PeT obtained by Mueller matrix imaging polarimetry at 550 nm.

As heterochiral domains (e.g., Figure 3) are differentially sensitive to left and right circularly polarized light by a mechanism that depends only on the dielectric susceptibility of the components—no magnetic dipole moments are required—the differential sensitivity of left and right circular polarized light in twisted semiconductor films may lead to strong differential photoconductivity dependent upon the polarization state of light. Moreover, because the orientation of twisted crystals is modulated systematically with respect to the film surface, there are a greater number of excited state transition dipole moments that may be accessed simultaneously or selectively with linearly polarized light.

OFET Measurements. PyT is semiconducting, with the measured mobilities of single crystals (derived from the transit times) of 2.6 cm²V⁻¹ s⁻¹ for electrons and 2.3 cm²V⁻¹ s⁻¹ for holes.⁴⁶ Later, researchers reported its anisotropic carrier mobility in which the donor-acceptor stacking direction is the dominant direction for hole mobility, orders of magnitude larger than that for electron mobility, while in the b-direction there is no appreciable differences between the carriers. 47-49 Nevertheless, the transient signals were always surprisingly too large to be taken. 46 To evaluate the electrical properties of CTCs at steady state, OFETs with a bottom-gate bottomcontact configuration were fabricated. The channel length (L)was 100 μ m and the width (W) was approximately 1 mm. Straight and twisted crystals were grown from the melt on the devices with the growth direction parallel to the current flow from the drain to the source, and three samples were prepared for each morphology.

OFETs prepared from crystals of PhT and PyT grown in a glovebox in a nitrogen gas environment did not show an apparent difference in mobility, indicating that oxidation ought not preclude measurements on samples prepared under ambient conditions. Our attempts to fabricate OFETs for PeT were unsuccessful because of its decomposition above melting point \sim 270 °C.

Figure 4 shows the current between the source and drain electrodes, I_{DS} , as a function of gate-source voltage (V_{GS}) at

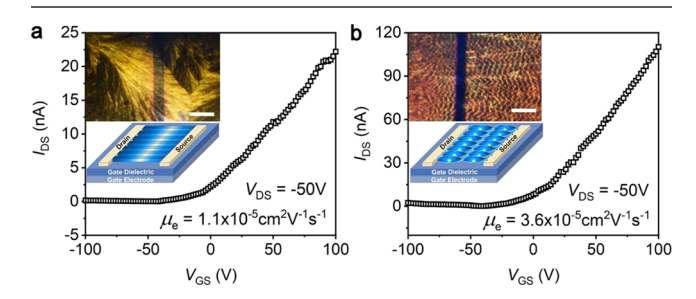


Figure 4. Current–voltage (I-V) characteristics of (a) straight PyT ($W = 2000 \ \mu \text{m}$) and (b) twisted PyT ($W = 3000 \ \mu \text{m}$). Gate dielectric capacitance per unit area $C_i = 1.06 \times 10^{-8} \ \text{F/cm}^2$. Scale bar = 200 μm .

constant drain-source voltage $V_{\rm DS}=-50~{\rm V}$ for straight and twisted PyT devices. The correlated electron mobilities for three straight and three twisted PyT devices are summarized in Table S3. PyT transistors with twisted crystals yielded an average electron mobility of $(3.2\pm0.5)\times10^{-5}~{\rm cm^2V^{-1}~s^{-1}}$, around three times higher than those with straight crystals, $(1.1\pm0.1)\times10^{-5}~{\rm cm^2V^{-1}~s^{-1}}$. A fourfold enhancement was obtained for the electron mobility of PhT, $(1.7\pm0.7)\times10^{-5}$ and $(6.8\pm1.2)\times10^{-5}~{\rm cm^2V^{-1}~s^{-1}}$ for straight and twisted crystals, respectively (Figure S7, Table S3).

Electronic Structure Calculations. The difference in charge mobilities between straight and twisted crystals was evaluated computationally based on DFT. Such calculations, albeit on individual crystals, serve as a baseline interpreting the differences in mobilities of polycrystalline films with straight and twisted crystals. For three selected CTCs, PhT, PyT and PeT, the large differences between the ionization potential of donors (IP_D) and electron affinity of acceptors (EA_A), 3.28–4.23 eV (Figure S8), indicate neutral CTCs rather than ionic CTCs. The following calculation focuses on PyT, consistent with OFET measurements presented above. The calculation results for PhT and PeT are shown in the Supporting Information.

Anisotropic carrier mobilities in straight crystals. According to first principles quantum mechanics calculations and Marcus—Hush theory, 50,51 we simulated the charge mobilities in straight crystals based on their geometries from crystallographic information files (Supporting Information CIF files). Many π -conjugated molecules crystallize into a layered herringbone packing motif, $^{52-54}$ which provides 2D transport only within the basal stacked organic layers, while transport between layers is less efficient. In this case, the carrier mobility can be calculated as eq 1

$$\mu_{\phi} = \frac{e}{2k_{\rm B}T} \sum_{i} r_i^2 W_i P_i \cos^2 \gamma_i \cos^2(\theta_i - \phi)$$
(1)

where e and $k_{\rm B}$ are the elementary charge and Boltzmann constant, respectively, and temperature T=300 K. The index, i, represents a specific hopping path with distance r_i (centroid-to-centroid). γ_i is the angle between the hopping path and the bottom X-Y plane, θ_i is the angle of the projected hopping path on the X-Y plane relative to the reference X axis, ϕ is the

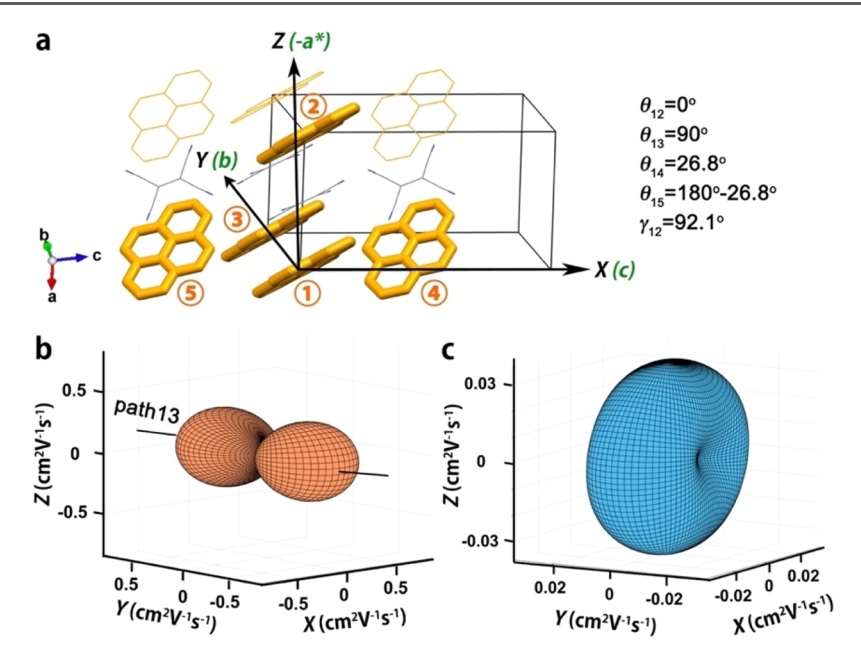


Figure 5. (a) Hopping paths 12, 13, 14, and 15 of PyT in the orthogonal coordinate basis $\{X, Y, Z\}$ and crystallographic system $\{a, b, c\}$. Simulated anisotropic (b) hole and (c) electron mobilities in straight PyT crystals.

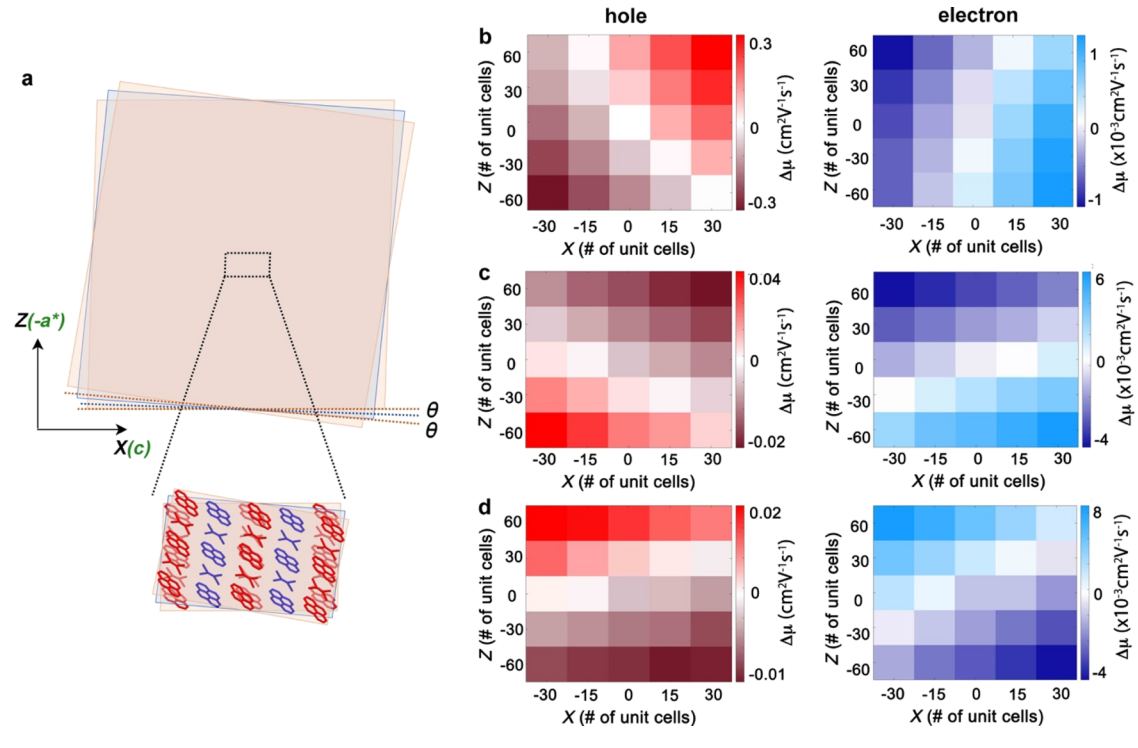


Figure 6. Schematic twisting and electronic properties of the PyT crystal after twisting in the orthogonal basis $\{X, Y, Z\}$ and averaging over the induced heterogeneity. (a) Three adjacent layers sequentially misoriented by $\theta = 0.01^{\circ}$ along <010>. The rotation angle is exaggerated for clarity. Change of hole and electron mobilities $\Delta\mu$ along hopping path (b) 13, (c) 14, and (d) 15 at 25 evenly distributed points within the twisted PyT superlattice compared with straight models.

orientation angle of the projected transistor channel on the X-Y plane to the reference X axis (Figure S9). $P_i = W_i/\sum_i W_i$ is the hopping probability. The hopping rate W_i is calculated from Marcus—Hush theory 50,51,55 as eq 2

$$W_{i} = \frac{t_{i}^{2}}{h} \left(\frac{\pi}{\lambda k_{\rm B}T}\right)^{1/2} \exp\left(-\frac{\lambda}{4k_{\rm B}T}\right) \tag{2}$$

where h is the Planck constant, λ is the reorganization energy, and t_i is the transfer integral along the hopping path i, defined in Supporting Information.

Figure 5a illustrates four hopping paths for PyT in a special orthogonal coordinate basis $\{X, Y, Z\}$ with $X \parallel c$, $Y \parallel b$, and $Z \parallel a^*$, including i = 12 along the donor—acceptor—donor stacking direction (a-axis) and the direct overlap between the closest donor and acceptor molecules (i = 13, 14 and 15). Transfer

integrals t_i and hopping rates W_i along each hopping path i are summarized in Table S4. Comparable transfer integrals can be found along four non-coplanar hopping paths, indicating 3D charge transport, not confined to single directions or layers, in agreement with the large band dispersion along Γ B, Γ Y, and Γ Z directions in electronic band structures (Figure S10). Since eq 1 cannot describe charge transport of our CTCs along non-coplanar hopping paths, it was modified to eq 3 by introducing the orientation angle δ of the transistor channel relative to the X-Y plane (Figure S9).

$$\mu_{\phi,\delta} = \frac{e}{2k_{\rm B}T} \sum_{i} r_i^2 W_i P_i (\cos \gamma_i \cos(\theta_i - \phi) + \sin \gamma_i \sin \delta)^2$$
(3)

If $\delta = 0$, then eq 3 reduces to eq 1. As shown in Figure 5a, the angles of hopping paths 13, 14, and 15 to the reference X axis θ_i are 90°, 26.8°, and 180°-26.8°, respectively. When hopping path 12 is projected on the X-Y plane, it is parallel to the reference X axis, and the angle γ_{12} with respect to X-Y plane is equal to the crystallographic β angle, 92.1°. eq 3 with transfer integrals t_i in Table S4 and reorganization energies in Table S5, leads to the hole and electron mobility orientation functions. The simulations show strongly anisotropic hole and electron mobilities of straight PyT crystals (Figure 5b,c). The hole mobilities along the X and Y axes are higher than those along other directions, but smallest along Z. Hopping paths 13, 14, and 15 are located inside the X-Y layer and thus do not contribute to the transport along the Z axis. The electron mobilities are the largest along the Z axis, $0.034 \text{ cm}^2\text{V}^{-1} \text{ s}^{-1}$. This is because the strong donor-acceptor π - π interactions favor hopping from donors to acceptors, consistent with the largest electron transfer integral along path 12 (Table S4). PhT and PeT also show similar anisotropic mobilities, but slightly different distribution of hole mobilities due to the varied structures of donors (Figure S11).

Charge carrier mobility, μ [cm² V⁻¹ s⁻¹], the quality that relates the average drift velocity of charge carriers, ν [cm·s⁻¹], to an applied electric field, E [V·cm⁻¹], is a distinguishing characteristic of semiconductors. Carrier mobility therefore can be expressed as a second-rank tensor: 56,57 $\nu_i = \mu_{ij}E_j$. The diagonal values μ_{ii} give the mobility along three axes in the orthogonal coordinate basis $\{X, Y, Z\}$. The elements of hole and electron mobility tensors μ_{ij} for three CTCs are shown in Table S6, and that of diagonalized tensors μ_{ij} in Table S7.

Simulated carrier mobilities in twisted crystals. For twisted crystals, mobility simulations must consider the transformation of atomic coordinates consistent with the twist, small on the molecular scale. The fiber elongation direction in twisted PyT crystals was determined experimentally as the crystallographic b-axis, which is parallel to the Y axis and the hopping path 13. Thus, twisting-relative positions of molecules inside the X-Z plane should not be affected and the charge transport will not change along hopping path 12, but change along 13, 14, and 15. We built a superlattice composed of three layers perpendicular to the fiber elongation direction b-axis (the first and second layer for the calculation of hopping paths 14 and 15, and the first and third layers for path 13) to evaluate the carrier mobilities in twisted fibers, as shown in Figure 6a. The twisting model requires: (1) the rotation angle θ between two adjacent layers and (2) the size of supercell, i.e., number of unit cells in a fiber cross section.

The rotation angle θ between two adjacent layers was chosen based on the measured distance needed for the fiber to

rotate by 180°, the pitch $P\approx 20-50~\mu{\rm m}$ in twisted PyT crystals. The corresponding rotation angle $\theta=\pi/P=0.004-0.01^\circ/{\rm distance}$ between two adjacent layers (~3.6 Å) along <010>. The upper limit of $\theta=0.01^\circ/{\rm 3.6}$ Å was chosen for further calculation. Fibers in twisted crystals with comparable pitches have cross sectional radii of $0.01-1~\mu{\rm m}^{58}$, thus the cross section of $50-200~{\rm nm}$ is a natural choice for simulations. However, the shear strain is assumed not to exceed the yield strain of $\gamma_{\rm max}<0.02$ (assuming high temperature $T/T_{\rm m}>0.65$). In twisted crystals, the maximum value corresponds to the fiber radius $r=\gamma_{\rm max}/\theta\approx 50~{\rm nm}$. For $r=50~{\rm nm}$, the side of the superlattice is 100 nm. The PyT lattice constant $c=14.2~{\rm \AA}$, so the number of unit cells along X (or c) is 100 nm/14.2 Å \approx 70. A similar estimate for Z (or $-a^*$) axis leads to 125 cells. The same supercell sizes (70×125) were chosen for PhT and PeT.

The calculation of 70×125 crystallographic unit cells in each supercell requires significant computational time. Therefore, we sampled 25 evenly distributed points and calculated the average mobilities along each hopping path. As shown in Figure 6, the supercell displacement between dimers along path 13, 14, and 15 increases with the distance from the rotation axis. The greater the displacement, the greater the change in carrier mobility. The carrier mobilities of twisted PyT crystals were calculated by combining results for hopping paths 13, 14, and 15 with the results for hopping path 12 (same as for straight crystals). The slight difference of the mobility in twisted supercells compared to straight crystals can be detected by comparing the mobility tensors (Tables S6 and S7). In particular, twisting $(0.01^{\circ}/3.6 \text{ Å})$ leads to an increase in the electron mobility of 25% along growth direction <010>.

Modest increases were also obtained for PhT and PeT (Figures S12 and S13, Tables S6 and S7). After twisting by 0.01° along the fiber elongation direction <010>, the average hole mobility of PhT slightly increased by 1%, and the electron mobility increased by 14%. Twisted PeT showed a 7% increase in hole mobility and a 13% increase in electron mobility along growth direction <100>. The trends among different CTCs predicted by our DFT calculations show that twisting by a small angle 0.01° between two adjacent layers can generally enhance the computed carrier mobilities but slightly.

DISCUSSION

Why are so many small molecular crystals twisted, 3,4,59 and why are mixed-stacking CTCs even more prone to form twisted fibrils? The first question resists one answer, or one mechanism. While large twisted crystals can be pulled from the ground,60 most twisted crystals are associated with slender fibrils.³ This, at the very least, satisfies mechanical intuition; it is easier to twist a crystal that is narrow in cross section and one that is thin. The torsion constant, while dependent on the shape of the cross section is roughly proportional to the inverse fourth power of the radius. However, the phrase "twisted crystal" can be misleading. If something has been twisted, it implies that there was something straight to begin with. However, when crystals are at the nanoscale, they need not conform to a lattice, they need not have long range translational symmetry. Simulations⁶¹ and mechanical considerations^{62,63} suggest that crystals may accommodate some frustration to continue to grow, thereby approximating a familiar crystal. Only molecules that conform to a lattice can be assembled from a semi-infinite number of molecules. The tension is manifest as needle-like crystals that twist at their tips,

while untwisting as they accommodate molecules that serve to thicken the needle laterally. ^{2,58} Twisting frustrates lateral assembly. In other cases, twisting is a consequence of the association of misaligned lamellae. ^{64,65} More generally, unbalanced surface stresses may be consequential in thin ribbons of high polymers. ⁶⁶ Strain because of inhomogeneities of crystallization additives/impurities may also play a role. The second question in the first sentence of this paragraph depends, somewhat, on a clear answer to the first. Whether or not the commonalities of the mixed-stack crystal structures and morphologies underlying the increased frequency in twisting remain to be established.

In a recent paper, researchers described a twisted CTC crystal composed of pyrene and DTTCNQ (4,8-bis-(dicyanomethylene)-4,8-dihydrobenzo[1,2-b:4,5-b']-dithiophene) deposited from solution.⁶⁷ Individual twisted helicoids were described, as in refs 31, 37. This is consistent with the propensity of twisting in CTCs describe here. Moreover, the pyrene-DTTCNQ untwisted on thickening, as we have previously described for other compounds.^{2,68} Our work here by contrast focuses exclusively on growth from melts.

DFT calculations and OFET measurements of charge mobilities on straight and twisted crystals can be evaluated in reference to the literature on electromechanical effects in organic semiconductors. Given the necessity of flexibility in materials supporting plastic electronic components, researchers naturally have focused their attention on the consequences of charge transport in strained crystals.

Among the first, if not the first, study of this kind was a consequence strain induced in 6,13-bis-(triisopropylsilylethynyl)pentacene (TIPS-pentacene) by a solution shearing technique. Molecular π -systems were ostensibly squeezed more closely increasing hole mobilities⁶⁹ by as much as six times. Subsequently, rubrene crystals, a material with outstanding hole mobility, were analyzed in a bent configuration on a flexible transistor. The Later rubrene studies based on OFET measurements showed that the high mobility direction can be enhanced by nearly a factor of two with a small compressive strain of 1%.⁷¹ In a radical cation crystal, 9,10-bis(phenylethynyl)anthracene radical cation (BPEA+), four-probe measurements showed a slight decrease in conductivity from 2.68 to 2.43 S/cm. A recent attempt to develop a computational strategy to predict the effects of external deformation on the charge transport in organic semiconductors showed that consequences, as to be expected, are highly material-dependent, although changes typically arise in the modification of charge transfer integrals rather than changing lattice dynamics.⁷³ Most recently, a stunning 7-order of magnitude enhancement in conductivity was reported for bent coronene crystals, 74 a result in sharp contrast with the more modest changes described above. The frequency of contributions on the electromechanical analysis of organic semiconductors indicates that this is an inquiry likely to develop quickly in the near term, 75 and may come into focus in tandem with the development of the basic science of mechanically dynamic molecular crystals.⁷⁶

In the case of spontaneously twisted crystals of CTCs, no external forces were applied. Any strain maintained in the materials during growth is self-accommodated. DFT calculations on twisted crystals apply a 0.02% strain $(\gamma_{\text{max}} = r\theta)$ associated with lattice misorientation. It leads to changes of several percent in the HOMO/LUMO transfer integral and carrier mobility (Figure 6) dependent on the supercell

displacement. The greater the skewing of adjacent layers, the greater the change in carrier mobility, some parts of the rod with rising mobilities and some falling. The average effect on the supercell for the twist specified above is a slight increase (up to 25%) in the calculated mobilities of twisted crystals.

Nevertheless, the changes in charge mobility can be predicted in single twisted crystals, and thus far measured in ensembles of crystals in OFETs. While comparing single-crystalline objects in silico to polycrystalline films in the laboratory lacks a certain fidelity, the difference between calculated enhancement of mobility (several percent) is substantially lower than the measured enhancement (several hundred percent). To understand the substantial differences between computations on single twisted crystals and the mobilities measured for ensembles of twisted crystals in close contact, we will need to build a model of the conductance in networks of crystals in order to capture this difference in the future.

Also, OFET measurements only record electron transport for PhT and PyT instead of ambipolar transport as in DFT calculations. Because of the small size of crystal domains (\sim 1 μ m), charge transport is not only along the fiber axis lying from drain to source, but along more complex paths mediated by grain boundaries between crystallites (Figure S14). Based on DFT calculations, hole mobility along the Z axis is much smaller than those along other directions, also 2 orders of magnitude lower than electron mobility.

CONCLUSIONS

Binary CTCs composed of organic donors and acceptors lie at the heart of science of organic metals and semiconductors from which organic materials science more broadly emerged. These compounds have been studied as single crystals grown from solution, almost exclusively. However, a remarkable proportion of CTCs studied here, 23 of 41, crystallized as banded spherulites from the melt in which the optical rhythm was a signature of twisted radial fibrils. This statistical fact about the crystalline morphology of organic CTCs merits further attention.

Among twisted CTCs described herein, three 1:1 mixed-stack TCNE-based complexes with phenanthrene (PhT), with pyrene (PyT), and with perylene (PeT) were characterized by complete polarimetry, crystal structure characterizations, OFET measurements (for PhT and PyT), and DFT calculations in both straight and twisted configurations. Both single crystals and banded spherulites show linear dichroism in polarized light with strong light absorbance along the donor–acceptor π – π stacking direction.

OFETs demonstrate around 300% higher electron mobilities for twisted PhT and PyT crystals compared to straight ones, along the crystal growth directions <010>. Expectations for the differences in charge mobility between straight single crystals and the same structures in which a twist has been introduced were evaluated computationally. A procedure for computing the charge mobility in twisted crystals was developed based on DFT. Here, we derived a formula to describe the hole and electron mobilities in three dimensions, which can be expressed as second-rank tensors. DFT calculations for straight CTC crystal models built from crystallographic information files show anisotropic hole and electron transport, with the highest electron mobility along donor—acceptor π – π stacking directions. Moreover, bilayer supercells with a 0.01° rotation angle between adjacent layers around experimental twisting

axis were built to evaluate the theoretical mobilities of twisted crystals. The calculation of a supercell presents better hole (electron) mobilities, enhanced by 3% (14%) for PhT along <010>, 1% (25%) for PyT along <010>, and 7% (13%) for PeT along <100>.

The difference between theory and experiment likely originates from a complex organization of fibrils in polycrystal-line ensembles, where the nature of the innumerable interfaces is undoubtedly consequential. Such studies still lay the foundation of crystal morphology in high-performance flexible organic electronics and can help to introduce novel high-performance applications.

■ EXPERIMENTAL SECTION

CTC Synthesis. All parent donors and acceptors in Figure 1 were purchased from Sigma-Aldrich and TCI America and used without further purification. CTCs were synthesized by mixing solutions of the donors and acceptors and precipitating single crystals by solvent evaporation. ⁸⁰ All combinations studied (except for the CTCs that decomposed before melting) are reported in Table S1.

Crystal Growth. Melt crystallization was performed by sandwiching several milligrams of CTCs between a glass microscope slide and coverslip. Upon melting, the material formed thin, $1-5~\mu m$, films. These crystallized between the melting points, $T_{\rm m}$, and room temperature using a hot stage, Kofler bench, or sandwiching between two metal blocks. For most systems, the crystals formed within 5 s. All CTCs were crystallized without additives and with ca. 10 wt % damar gum resin. Twist generally occurs at higher undercoolings. The crystals were then surveyed in polarized light or between two polarizers in a petrographic microscope. We counted those instances in which there was tell-tale rhythmic progression of the absorbance and interference indicative of helicoidal twisting of fibrils.

OFET Fabrication and Electrical Characterization. For OFETs comprising straight or twisted crystals, a bottom-gate, bottom-contact structure was used, where the bottom gate consisted of highly doped silicon with 200 nm of thermally grown SiO₂ as the gate dielectric. Source and drain contacts were patterned by photolithography and deposited by thermal evaporation (4 nm Cr followed by 40 nm Au). Samples were then immersed in a 1 wt % solution of pentafluorobenzenethiophenol in anhydrous ethanol for 60 min followed by a 30-minute rinse in ethanol. Cleaned SiO₂/Si substrates were then exposed to UV-ozone for 10 min. The straight and twisted crystals on the OFET were processed as described in the Crystal Growth section. OFET measurements were performed using a Keithley 2636B system sourcemeter at room temperature.

Computational Methodology. The calculations of transfer integrals, reorganization energy, and mobility parameters were implemented using the DFT with the B3LYP functional and the 6-31G(d) basis set, using the Gaussian 16 package, ⁸¹ according to the general scheme of Bredas ^{52,82} among others. ^{50,51,83}

ASSOCIATED CONTENT

Supporting Information

The Supporting Information is available free of charge at https://pubs.acs.org/doi/10.1021/acs.chemmater.1c04003.

Experimental details, computational details, and crystal data. Crystallographic data for the structures reported in this article have been deposited at the Cambridge Crystallographic Data Centre (CCDC), under deposition nos. 2,107,190–2,107,195 (PDF)

AUTHOR INFORMATION

Corresponding Authors

Stephanie S. Lee – Department of Chemistry and Molecular Design Institute, New York University, New York, New York 10003, United States; orcid.org/0000-0003-0964-6353; Email: stephlee@nyu.edu

Alexander G. Shtukenberg — Department of Chemistry and Molecular Design Institute, New York University, New York, New York 10003, United States; orcid.org/0000-0002-5590-4758; Email: shtukenberg@mail.ru

Bart Kahr — Department of Chemistry and Molecular Design Institute, New York University, New York, New York 10003, United States; orcid.org/0000-0002-7005-4464; Email: bart.kahr@nyu.edu

Authors

Yongfan Yang — Department of Chemistry and Molecular Design Institute, New York University, New York, New York 10003, United States; orcid.org/0000-0003-3511-9733

Yuze Zhang — Department of Chemical Engineering and Materials Science, Stevens Institute of Technology, Hoboken, New Jersey 07030, United States

Chunhua T. Hu − Department of Chemistry and Molecular Design Institute, New York University, New York, New York 10003, United States; orcid.org/0000-0002-8172-2202

Mengmeng Sun – Department of Chemistry and Molecular Design Institute, New York University, New York, New York 10003, United States

Sehee Jeong — Department of Chemistry and Molecular Design Institute, New York University, New York, New York 10003, United States

Complete contact information is available at: https://pubs.acs.org/10.1021/acs.chemmater.1c04003

Author Contributions

Y.Y., A.S. and B.K. conceived the idea and design the experiments. Y.Y. and M.S. performed the synthesis and melt crystallization of charge transfer complexes. C.T.H. performed the single-crystal analysis. Y.Y., Y.Z. and S.J. carried out the measurement of carrier mobility on the transistors. Y.Y. did the DFT calculations. B.K. and S.S.L. directed the project. Y.Y., B.K., A.S. and S.S.L. wrote the manuscript, with input from all authors.

Notes

The authors declare no competing financial interest.

ACKNOWLEDGMENTS

This work was primarily supported by the National Science Foundation DMR-2003968 and secondarily by the New York University Materials Research Science and Engineering Center (MRSEC) program of the National Science Foundation under award number DMR-1420073. We thank Dr. Shenglong Wang for his help with Gaussian calculation on high-performance computing (HPC) and St. John Whittaker for his help with optical characterization.

REFERENCES

- (1) Bernauer, F. Gedrillte; Kristalle: Gebruder Bornträger, Berlin, 1929.
- (2) Shtukenberg, A. G.; Freudenthal, J.; Kahr, B. Reversible twisting during helical hippuric acid crystal growth. *J. Am. Chem. Soc.* **2010**, 132, 9341–9349.
- (3) Shtukenberg, A. G.; Punin, Y. O.; Gujral, A.; Kahr, B. Growth actuated bending and twisting of single crystals. *Angew. Chem., Int. Ed.* **2014**, 53, 672–699.

- (4) Shtukenberg, A. G.; Zhu, X.; Yang, Y.; Kahr, B. Common occurrence of twisted molecular crystal morphologies from the melt. *Cryst. Growth Des.* **2020**, 20, 6186–6197.
- (5) Cui, X.; Rohl, A. L.; Shtukenberg, A. G.; Kahr, B. Twisted aspirin crystals. *J. Am. Chem. Soc.* **2013**, *135*, 3395–3398.
- (6) Shtukenberg, A. G.; Tan, M.; Vogt-Maranto, L.; Chan, E. J.; Xu, W.; Yang, J.; Tuckerman, M. E.; Hu, C. T.; Kahr, B. Melt crystallization for paracetamol polymorphism. *Cryst. Growth Des.* **2019**, *19*, 4070–4080.
- (7) Yang, J.; Hu, C. T.; Zhu, X.; Zhu, Q.; Ward, M. D.; Kahr, B. DDT polymorphism and the lethality of crystal forms. *Angew. Chem., Int. Ed.* **2017**, *56*, 10165–10169.
- (8) Yang, J.; Erriah, B.; Hu, C. T.; Reiter, E.; Zhu, X.; Lopez-Mejias, V.; Carmona-Sepulveda, I. P.; Ward, M. D.; Kahr, B. A deltamethrin crystal polymorph for more effective malaria control. *Proc. Natl. Acad. Sci. U. S. A.* **2020**, *117*, 26633–26638.
- (9) Zhu, Q.; Shtukenberg, A. G.; Carter, D. J.; Yu, T. Q.; Yang, J. X.; Chen, M.; Raiteri, P.; Oganov, A. R.; Pokroy, B.; Polishchuk, I.; Bygrave, P. J.; Day, G. M.; Rohl, A. L.; Tuckerman, M. E.; Kahr, B. Resorcinol crystallization from the melt: a new ambient phase and new "riddles". J. Am. Chem. Soc. 2016, 138, 4881–4889.
- (10) Shtukenberg, A. G.; Zhu, Q.; Carter, D. J.; Vogt, L.; Hoja, J.; Schneider, E.; Song, H.; Pokroy, B.; Polishchuk, I.; Tkatchenko, A.; Oganov, A. R.; Rohl, A. L.; Tuckerman, M. E.; Kahr, B. Powder diffraction and crystal structure prediction identify four new coumarin polymorphs. *Chem. Sci.* **2017**, *8*, 4926–4940.
- (11) Wudl, F.; Wobschall, D.; Hufnagel, E. J. Electrical conductivity by the bis(1,3-dithiole)-bis(1,3-dithiolium) system. *J. Am. Chem. Soc.* **1972**, *94*, *670*–*672*.
- (12) Ferraris, J.; Cowan, D. O.; Walatka, V. T.; Perlstein, J. H. Electron transfer in a new highly conducting donor—acceptor complex. *J. Am. Chem. Soc.* **1973**, *95*, 948–949.
- (13) Goetz, K. P.; Vermeulen, D.; Payne, M. E.; Kloc, C.; McNeil, L. E.; Jurchescu, O. D. Charge-transfer complexes: new perspectives on an old class of compounds. *J. Mater. Chem. C* **2014**, *2*, 3065–3076.
- (14) Geng, H.; Zheng, X.; Shuai, Z.; Zhu, L.; Yi, Y. Understanding the charge transport and polarities in organic donor—acceptor mixed-stack crystals: molecular insights from the super-exchange couplings. *Adv. Mater.* **2015**, *27*, 1443–1449.
- (15) Diao, Y.; Shaw, L.; Bao, Z.; Mannsfeld, S. C. B. Morphology control strategies for solution-processed organic semiconductor thin films. *Energy Environ. Sci.* **2014**, *7*, 2145–2159.
- (16) Liu, S.; Wang, W. M.; Briseno, A. L.; Mannsfeld, S. C. B.; Bao, Z. Controlled deposition of crystalline organic semiconductors for field-effect-transistor applications. *Adv. Mater.* **2009**, *21*, 1217–1232.
- (17) Virkar, A. A.; Mannsfeld, S.; Bao, Z.; Stingelin, N. Organic semiconductor growth and morphology considerations for organic thin-film transistors. *Adv. Mater.* **2010**, *22*, 3857–3875.
- (18) Diao, Y.; Tee, B. C. K.; Giri, G.; Xu, J.; Kim, D. H.; Becerril, H. A.; Stoltenberg, R. M.; Lee, T. H.; Xue, G.; Mannsfeld, S. C. B.; Bao, Z. Solution coating of large-area organic semiconductor thin films with aligned single-crystalline domains. *Nat. Mater.* **2013**, *12*, 665–671.
- (19) Xia, Y.; Li, R.; Tsai, E.; He, Y.; Liu, T.; Zhao, X.; Gu, K.; Meng, H.; Loo, Y. L. Solvent-free coating of organic semiconductor membranes with centimetric crystalline domains. *Adv. Electron. Mater.* **2021**, 7, No. 2000792.
- (20) Zhao, Y.; Zhao, X.; Roders, M.; Gumyusenge, A.; Ayzner, A. L.; Mei, J. Melt-processing of complementary semiconducting polymer blends for high performance organic transistors. *Adv. Mater.* **2017**, *29*, No. 1605056.
- (21) Qiu, L.; Xu, Q.; Chen, M.; Wang, X.; Wang, X.; Zhang, G. Low-temperature melt processed polymer blend for organic thin-film transistors. *J. Mater. Chem.* **2012**, 22, 18887–18892.
- (22) Sidletskiy, O. T.; Lisetski, L. N.; Malikov, V. Y.; Stadnik, P. E.; Panikarskaya, V. D.; Budakovsky, S. V. Experimental and theoretical studies of charge transfer complexes in chloranil-doped molecular crystal melts. *Funct. Mater.* **2002**, *9*, 721.

- (23) Gupta, R. K.; Singh, S. K.; Singh, R. A. Some physicochemical studies on organic eutectics. *J. Cryst. Growth* **2007**, *300*, 415–420.
- (24) Gupta, R. K.; Singh, R. A. Thermochemical and microstructural studies on binary organic eutectics and complexes. *J. Cryst. Growth* **2004**, 267, 340–347.
- (25) Carr, S.; Massatt, D.; Fang, S.; Cazeaux, P.; Luskin, M.; Kaxiras, E. Twistronics: Manipulating the electronic properties of twodimensional layered structures through their twist angle. *Phys. Rev.* B **2017**, 95, No. 075420.
- (26) Cao, Y.; Rodan-Legrain, D.; Rubies-Bigorda, O.; Park, J. M.; Watanabe, K.; Taniguchi, T.; Jarillo-Herrero, P. Tunable correlated states and spin-polarized phases in twisted bilayer-bilayer graphene. *Nature* **2020**, *5*83, 215–220.
- (27) Cao, Y.; Fatemi, V.; Demir, A.; Fang, S.; Tomarken, S. L.; Luo, J. Y.; Sanchez-Yamagishi, J. D.; Watanabe, K.; Taniguchi, T.; Kaxiras, E.; Ashoori, R. C.; Jarillo-Herrero, P. Correlated insulator behaviour at half-filling in magic-angle graphene superlattices. *Nature* **2018**, *556*, 80–84.
- (28) Yankowitz, M.; Chen, S. W.; Polshyn, H.; Zhang, Y. X.; Watanabe, K.; Taniguchi, T.; Graf, D.; Young, A. F.; Dean, C. R. Tuning superconductivity in twisted bilayer graphene. *Science* **2019**, 363, 1059–1064.
- (29) Lu, X. B.; Stepanov, P.; Yang, W.; Xie, M.; Aamir, M. A.; Das, I.; Urgell, C.; Watanabe, K.; Taniguchi, T.; Zhang, G. Y.; Bachtold, A.; MacDonald, A. H.; Efetov, D. K. Superconductors, orbital magnets and correlated states in magic-angle bilayer graphene. *Nature* **2019**, *574*, 653–657.
- (30) Morell, E. S.; Correa, J. D.; Vargas, P.; Pacheco, M.; Barticevic, Z. Flat bands in slightly twisted bilayer graphene: Tight-binding calculations. *Phys. Rev. B* **2010**, *82*, No. 121407.
- (31) Ikemoto, I.; Kuroda, H. The refinement of the crystal Structure of the pyrene-tetracyanoethylene complex. *Acta Crystallogr. B* **1968**, 24, 383–387.
- (32) Ikemoto, I.; Yakushi, K.; Kuroda, H. The refinement of crystal structure of perylene-tetracyanoethylene complex. *Acta Cryst.* **1970**, 26, 800–806.
- (33) McKinnon, J. J.; Jayatilaka, D.; Spackman, M. A. Towards quantitative analysis of intermolecular interactions with Hirshfeld surfaces. *Chem. Commun.* **2007**, 3814–3816.
- (34) Mandal, A.; Choudhury, A.; Sau, S.; Iyer, P. K.; Mal, P. Exploring ambipolar semiconductor nature of binary and ternary charge-transfer cocrystals of triphenylene, pyrene, and TCNQ. *J. Phys. Chem. C* **2020**, *124*, 6544–6553.
- (35) Kuroda, H.; Amano, T.; Ikemoto, I.; Akamatu, H. Charge-transfer interaction in tetracyanoethylene complexes of pyrene and naphthalene. J. Am. Chem. Soc. 1967, 89, 6056–6063.
- (36) Wynne, K.; Reid, G. D.; Hochstrasser, R. M. Vibrational coherence in electron transfer: the tetracyanoethylene-pyrene complexes. *J. Chem. Phys.* **1996**, *105*, 2287–2297.
- (37) Maleki, A.; Seidali, Z.; Zakerhamidi, M.; Majles Ara, M. Dichroic ratio and order parameters of some Sudan dyes doped in nematic liquid crystalline matrix. *Optik* **2015**, *126*, 5473–5477.
- (38) Fukuoka, E.; Makita, M.; Nakamura, Y. Glassy state of pharmaceuticals. V. relaxation during cooling and heating of glass by differential scanning calorimetry. *Chem. Pharm. Bull.* **1991**, 39, 2087–2090.
- (39) Freudenthal, J. H.; Hollis, E.; Kahr, B. Imaging chiroptical artifacts. *Chirality* **2009**, *21*, 20–27.
- (40) Cui, X.; Shtukenberg, A.; Freudenthal, J.; Nichols, S. M.; Kahr, B. Circular birefringence in banded spherulites. *J. Am. Chem. Soc.* **2014**, *136*, 5481–5490.
- (41) Cui, X.; Nichols, S. M.; Arteaga, O.; Freudenthal, J.; Paula, F.; Shtukenberg, A. G.; Kahr, B. Dichroism in helicoidal crystals. *J. Am. Chem. Soc.* **2016**, *138*, 12211–12218.
- (42) Arteaga, O. B.; Kahr, B. Mueller matrix polarimetry of bianisotropic materials. *J. Opt. Soc. Am. B* **2019**, *36*, F72–F83.
- (43) Tan, M.; Jiang, W.; Martin, A. T.; Shtukenberg, A. G.; McKee, M. D.; Kahr, B. Polarized light through polycrystalline vaterite helicoids. *Chem. Commun.* **2020**, *56*, 7353–7356.

- (44) Zhang, C.; Wang, X.; Qiu, L. Circularly polarized photo-detectors based on chiral materials: A review. *Front. Chem.* **2021**, *9*, No. 711488.
- (45) Wade, J.; Hilfiker, J. N.; Brandt, J. R.; Liirò-Peluso, L.; Wan, L.; Shi, X.; Salerno, F.; Ryan, S. T. J.; Schöche, S.; Arteaga, O.; Javorfi, T.; Siligardi, G.; Wang, C.; Amabilino, D. B.; Beton, P. H.; Campbell, A. J.; Fuchter, M. J. Natural optical activity as the origin of the large chiroptical properties in π -conjugated polymer thin films. *Nat. Commun.* **2020**, *11*, 6137.
- (46) Tobin, M. C.; Spitzer, D. P. Electrical properties of single-crystals of pyrene-tetracyanoethylene charge-transfer complex. *J. Chem. Phys.* **1965**, *42*, 3652–3658.
- (47) Kaino, H.; Sato, H. Transit-time measurements of photocarriers in vapor-grown pyrene-tone single-crystals. *J. Phys. Soc. Jpn.* **1978**, *44*, 685–686.
- (48) Kaino, H. Transient photocurrents in pyrene-tcne single-crystals. J. Phys. Soc. Jpn. 1974, 36, 1500.
- (49) Kaino, H. Transient photocurrents in pyrene-tcne single-crystals. 2. Anisotropy of Drift Mobility. *J. Phys. Soc. Jpn.* **1976**, 41, 570–573.
- (50) Marcus, R. A. Electrostatic free energy and other properties of states having nonequilibrium polarization. 1. *J. Chem. Phys.* **1956**, 24, 979–989.
- (51) Hush, N. S. Adiabatic rate processes at electrodes. 1. energy-charge relationships. *J. Chem. Phys.* **1958**, *28*, 962–972.
- (52) Zhu, L. Y.; Yi, Y. P.; Li, Y.; Kim, E. G.; Coropceanu, V.; Bredas, J.-L. Prediction of remarkable ambipolar charge-transport characteristics in organic mixed-stack charge-transfer crystals. *J. Am. Chem. Soc.* **2012**, *134*, 2340–2347.
- (53) Coropceanu, V.; Cornil, J.; da Silva Filho, D. A.; Olivier, Y.; Silbey, R.; Bredas, J.-L. Charge transport in organic semiconductors. *Chem. Rev.* **2007**, *107*, 926.
- (54) Wen, S. H.; Li, A.; Song, J. L.; Deng, W. Q.; Han, K. L.; Goddard, W. A. First-principles investigation of anistropic hole mobilities in organic semiconductors. *J. Phys. Chem. B* **2009**, *113*, 8813–8819.
- (55) Kubo, R.; Toyozawa, Y. Application of the method of generating function to radiative and non-radiative transitions of a trapped electron in a crystal. *Prog. Theor. Phys.* **1955**, *13*, 160–182.
- (56) Lovett, D. R. Tensor properties of crystals, 2nd ed.; Institute of Physics Pub.: Philadelphia, 1999; p xiii, 166.
- (57) Nye, J. F. Physical properties of crystals: their representation by tensors and matrices. 1st published in pbk. with corrections, 1984. ed.; Clarendon Press; Oxford University Press: Oxford Oxfordshire, New York, 1984.
- (58) Shtukenberg, A. G.; Gujral, A.; Rosseeva, E.; Cui, X. Y.; Kahr, B. Mechanics of twisted hippuric acid crystals untwisting as they grow. *CrystEngComm* **2015**, *17*, 8817–8824.
- (59) Killalea, C. E.; Amabilino, D. B. Stereochemistry and twisted crystals. *Isr. J. Chem.* **2021**, *61*, 629–644.
- (60) Žorž, M. Quarz-Gwindel. Miner. Welt 2009, 20, 30-46.
- (61) Li, C.; Shtukenberg, A. G.; Vogt-Maranto, L.; Efrati, E.; Raiteri, P.; Gale, J. D.; Rohl, A. L.; Kahr, B. Why are some crystals straight? *J. Phys. Chem. C* **2020**, *124*, 15616–15624.
- (62) Haddad, A.; Aharoni, H.; Sharon, E.; Shtukenberg, A. G.; Kahr, B.; Efrati, E. Twist renormalization in molecular crystals driven by geometric frustration. *Soft Matter* **2019**, *15*, 116–126.
- (63) Efrati, E. Geometric frustration in molecular crystals. *Isr. J. Chem.* **2020**, *60*, 1185–1189.
- (64) Shtukenberg, A. G.; Drori, R.; Sturm, E.; Vidavsky, N.; Haddad, A.; Zheng, J.; Estroff, L.; Weissman, H.; Wolf, S. G.; Shimoni, E.; Li, C.; Fellah, N.; Efrati, E.; Kahr, B. Crystals of benzamide, the first polymorphous molecular compound, are helicoidal. *Angew. Chem., Int. Ed.* **2020**, *132*, 14701–14709.
- (65) Cajamarca, L.; Grason, G. M. Geometry of flexible filament cohesion: better contact through twisting? *J. Chem. Phys.* **2014**, *141*, 174904.
- (66) Crist, B.; Schultz, J. M. Polymer spherulites: A critical review. *Prog. Polym. Sci.* **2016**, *56*, 1–63.

- (67) Yang, C.; Luo, L.; Chen, J.; Yang, B.; Wang, W.; Wang, H.; Long, G.; Liu, G.; Zhang, J.; Huang, W. Helical mesoscopic crystals based on an achiral charge-transfer complex with controllable untwisting/breaking. *Chem. Commun.* **2021**, *57*, 10031–10034.
- (68) Li, C.; Shtukenberg, A. G.; Carter, D. J.; Cui, X.; Olson, I.; Rohl, A. L.; Gale, J. D.; Raiteri, P.; Kahr, B. Timoshenko bending and eshelby twisting predicted in molecular nanocrystals. *J. Phys. Chem. C* **2018**, *122*, 25085–25091.
- (69) Giri, G.; Verploegen, E.; Mannsfeld, S. C. B.; Atahan-Evrenk, S.; Kim, D. H.; Lee, S. Y.; Becerril, H. A.; Aspuru-Guzik, A.; Toney, M. F.; Bao, Z. Tuning charge transport in solution-sheared organic semiconductors using lattice strain. *Nature* **2011**, *480*, 504–508.
- (70) Elsner, J.; Giannini, S.; Blumberger, J. Mechanoelectric response of single-crystal rubrene from Ab initio molecular dynamics. *J. Phys. Chem. Lett.* **2021**, *12*, 5857–5863.
- (71) Choi, H. H.; Yi, H. T.; Tsurumi, J.; Kim, J. J.; Briseno, A. L.; Watanabe, S.; Takeya, J.; Cho, K.; Podzorov, V. A large anisotropic enhancement of the charge carrier mobility of flexible organic transistors with strain: a hall effect and Raman study. *Adv. Sci.* **2020**, *7*, No. 1901824.
- (72) Kwon, T.; Koo, J. Y.; Choi, H. C. Highly conducting and flexible radical crystals. *Angew. Chem., Int. Ed.* **2020**, *59*, 16436–16439
- (73) Landi, A.; Peluso, A.; Troisi, A. Quantitative prediction of the electro-mechanical response in organic crystals. *Adv. Mater.* **2021**, *33*, No. 2008049.
- (74) Chen, Y.; Chang, Z.; Zhang, J.; Gong, J. Bending for better: flexible organic single crystals with controllable curvature and curvature-related conductivity for customized electronic devices. *Angew. Chem., Int. Ed.* **2021**, *60*, 22424–22431.
- (75) Raghuwanshi, V.; Bharti, D.; Mahato, A. K.; Shringi, A. K.; Varun, I.; Tiwari, S. P. High performance flexible organic field-effect transistors with barium strontium titanate gate dielectric deposited at room temperature. *ACS Appl. Electron. Mater.* **2020**, *2*, 529–536.
- (76) Naumov, P.; Karothu, D. P.; Ahmed, E.; Catalano, L.; Commins, P.; Halabi, J. M.; Al-Handawi, M. B.; Li, L. The rise of dynamic crystals. *J. Am. Chem. Soc.* **2020**, *142*, 13256–13272.
- (77) Naumov, P.; Chizhik, S.; Panda, M. K.; Nath, N. K.; Boldyreva, E. Mechanically responsive molecular crystals. *Chem. Rev.* **2015**, *115*, 12440–12490.
- (78) Sato, O. Dynamic molecular crystals with switchable physical properties. *Nat. Chem.* **2016**, *8*, 644–656.
- (79) Saha, S.; Mishra, M. K.; Reddy, C. M.; Desiraju, G. R. From molecules to interactions to crystal engineering: Mechanical properties of organic solids. *Acc. Chem. Res.* **2018**, *51*, 2957–2967.
- (80) Dasari, R. R.; Wang, X.; Wiscons, R. A.; Haneef, H. F.; Ashokan, A.; Zhang, Y. D.; Fonari, M. S.; Barlow, S.; Coropceanu, V.; Timofeeva, T. V.; Jurchescu, O. D.; Bredas, J.-L.; Matzger, A. J.; Marder, S. R. Charge-transport properties of F(6)TNAP-based charge-transfer cocrystals. *Adv. Funct. Mater.* **2019**, *29*, No. 1904858.
- (81) Frisch, M. J.; Trucks, G. W.; Schlegel, H. B.; Scuseria, G. E.; Robb, M. A.; Cheeseman, J. R.; Scalmani, G.; Barone, V.; Petersson, G. A.; Nakatsuji, H.; Li, X.; Caricato, M.; Marenich, A. V.; Bloino, J.; Janesko, B. G.; Gomperts, R.; Mennucci, B.; Hratchian, H. P.; Ortiz, J. V.; Izmaylov, A. F.; Sonnenberg, J. L.; Williams-Young, D.; Ding, F.; Lipparini, F.; Egidi, F.; Goings, J.; Peng, B.; Petrone, A.; Henderson, T.; Ranasinghe, D.; Zakrzewski, V. G.; Gao, J.; Rega, N.; Zheng, G.; Liang, W.; Hada, M.; Ehara, M.; Toyota, K.; Fukuda, R.; Hasegawa, J.; Ishida, M.; Nakajima, T.; Honda, Y.; Kitao, O.; Nakai, H.; Vreven, T.; Throssell, K.; Montgomery, J. A., Jr.; Peralta, J. E.; Ogliaro, F.; Bearpark, M. J.; Heyd, J. J.; Brothers, E. N.; Kudin, K. N.; Staroverov, V. N.; Keith, T. A.; Kobayashi, R.; Normand, J.; Raghavachari, K.; Rendell, A. P.; Burant, J. C.; Iyengar, S. S.; Tomasi, J.; Cossi, M.; Millam, J. M.; Klene, M.; Adamo, C.; Cammi, R.; Ochterski, J. W.; Martin, R. L.; Morokuma, K.; Farkas, O.; Foresman, J. B.; Fox, D. J. Gaussian 16, Revision A.03; Gaussian Inc.: Wallingford, CT, 2016.
- (82) Bredas, J.-L.; Beljonne, D.; Coropceanu, V.; Cornil, J. Charge-transfer and energy-transfer processes in π -conjugated oligomers and polymers: A molecular picture. *Chem. Rev.* **2004**, *104*, 4971–5004.

(83) Zhang, Y. H.; Duan, Y. P.; Song, L. L.; Zheng, D. Y.; Zhang, M. X.; Zhao, G. J. Charge-transfer mobility and electrical conductivity of PANI as conjugated organic semiconductors. *J. Chem. Phys.* **2017**, 147, 114905.

